Eur. J. Mech. B - Fluids 19 (2000) 503–528

S0997-7546(00)00131-X/FLA

Turbulence control in wall jets

Martin Schober *, Hans-Hermann Fernholz

Hermann-Föttinger-Institut für Strömungsmechanik, Technische Universität Berlin, Straße des 17. Juni 135, 10623 Berlin, Germany

(Received 20 July 1999; revised 15 March 2000; accepted 22 March 2000)

Abstract – A new method for the control of mixing of a plane turbulent wall jet has been investigated. A thin wire, mounted in the vicinity of the wall-jet nozzle, changes the formation of the shear-layer structures in the early stages of the development of the wall jet. The wire is operated in two ways: (1) a still wire inhibits the natural shear layer roll-up and reduces the size of the turbulent structures and thereby the mixing; (2) a self-excited oscillating wire introduces large coherent structures and thereby enhances the mixing. The size of these structures does not depend on the shear-layer instability but rather on the wire frequency.

Measurements of the mean and fluctuating velocities have been performed with hot-wire anemometry as well as measurements of the skin friction by means of Preston tubes, surface fences and wall hot-wires. The Reynolds number based on the slot width was $Re_j = 10000$. © 2000 Éditions scientifiques et médicales Elsevier SAS

wall jet / shear layer / turbulence / control

1. Introduction

A wall jet is a flow that has features of both a boundary layer and a jet. Its main application lies with turbine blade cooling and high lift airfoils or flaps. These two technical applications already illustrate the opposed demands a wall jet is utilised for. In the former case it is desirable to prevent the cooling fluid from mixing with the ambient flow in order to maintain the protective layer as far downstream as possible, whereas in the latter case it is desirable to stimulate the mixing of the wall jet with the ambient flow. The aim of the present investigation is to influence the global characteristics of a turbulent wall jet, i.e. to manipulate the spreading rate and the skin friction.

The manipulation of free shear layers has been widely investigated (for instance Freymuth [1], Fiedler and Mensing [2], Ho and Huang [3]). It seems to be well established that the transverse momentum transport in turbulent shear- and mixing layers is largely determined by the motion of large scale coherent structures. The origin of these structures are the vortices generated by the shear-layer instability. Several stages of vortex pairing can significantly enlarge the size of the vortices. Even in fully developed turbulent shear layers, these coherent structures coexist with a fine-scale motion.

Katz, Horev and Wygnanski [4] and Zhou, Heine and Wygnanski [5] investigated the influence of acoustic excitation on the coherent structures of a plane wall-jet. Katz et al. [4] achieved a reduction of the skin friction (determined via the gradient of the velocity profile measured by hot-wire anemometry) of up to 30%, but only when forcing at large amplitudes of 20% of the wall-jet exit velocity. An increase of the skin friction has, however, not been observed. Zhou et al. [5] found that, as in free shear layers, the momentum exchange between the wall-jet and the surrounding fluid was largely dependent on these structures. The manipulation of the

* Correspondence and reprints; e-mail: schober@pi.tu-berlin.de

coherent structures therefore enabled us to manipulate the interaction between the wall jet and its surrounding fluid.

The manipulation of the coherent structures is commonly accomplished by the excitation of the shear-layer instability or its subharmonics. The size of the structures which can be stimulated by such a manipulation is always restricted to the limited bandwidth in which the shear layer amplifies disturbances. The amplification rate of disturbances with an excitation frequency outside this bandwidth will be small, and will not change the natural development of the flow.

Relatively little interest has been shown so far in methods introducing an additional passive device, such as a trip wire. Strykowski and Sreenivasan [6] suppressed the Kármán vortex street behind a cylinder by introducing a smaller cylinder into the wake of the main cylinder. Tong and Warhaft [7] reduced the spreading and the turbulence level in an axisymmetric jet by placing a thin ring immediately downstream of the nozzle of their wind-tunnel, and Rajagopalan and Antonia [8] reduced the turbulence in a plane mixing layer by means of a small cylinder. Schober and Fernholz [9] reported similar results for the case of a wall-jet. All these investigations utilise the wake introduced by a thin cylinder into a shear layer. The influence of such a wake on a wall-jet is the first topic of the present investigation.

Vandsburger and Ding [10] reported that an oscillating 'music' wire stimulated the energy transfer in a free shear layer. The wire was performing flow-induced vibrations, i.e. no external additional input was required. The influence of such an oscillating wire on a wall-jet is the second topic addressed here.

2. Experimental setup

Experiments have been carried out in a plane 2-dimensional wall-jet as shown in *figure 1*. The length of the slot was $B = 500$ mm and the Reynolds number based on the jet exit velocity u_j and the slot width $b = 8$ mm was $Re_j = 10000$, unless otherwise stated. At this Reynolds number the turbulent wall jet is self-preserving in

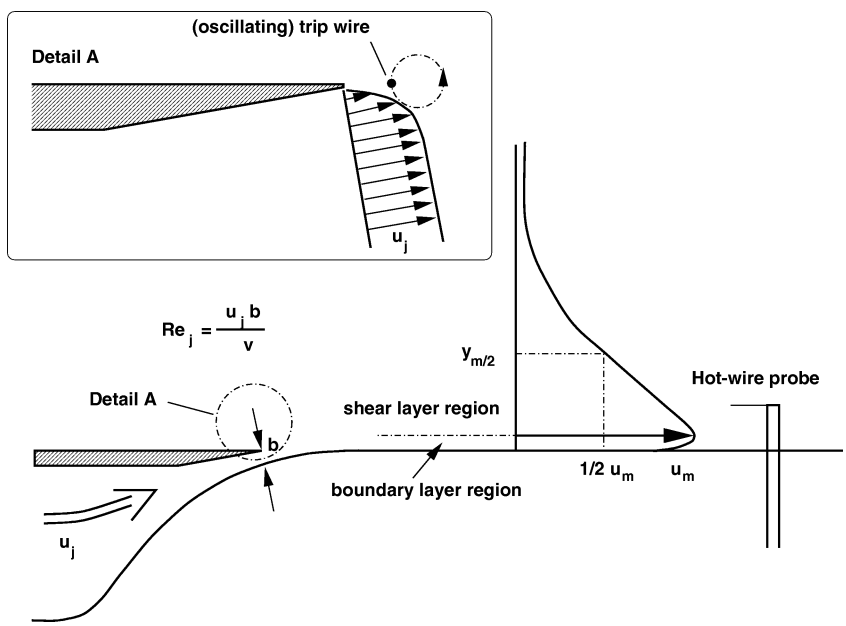

Figure 1. Experimental facility.

the region $40 \leqslant x/b \leqslant 150$ with respect to the mean and turbulence quantities, as has been shown for instance by Abrahamsson, Johansson and Löfdahl [11] and Schober [12].

Hot-wire velocity measurements were carried out to obtain mean and turbulence quantities as well as spectra. The hot-wire equipment consisted of IFA-100 constant temperature bridges with signal conditioners, a 12 bit AD-converter with sample and hold and an Atari microcomputer which controlled the AD-converter and the traverse gear. The single wire and X-wire probes had an active length of 0.50 mm with a length to diameter ratio of 200. The wires featured gold plated ends to minimise prong interference. Pressure measurements were made using MKS Baratron temperature compensated transducers with a resolution of 0.01 Pa and an accuracy of 0.15% of the reading. The skin friction was measured by means of Preston tubes, surface fences and wall hot wires. The latter two methods are independent of the so called logarithmic law of the wall, but need to be calibrated in a known flow. A more detailed description of these methods is found in Fernholz et al. [13]. All probes employed in this investigation have been manufactured at the Hermann-Föttinger-Institut.

The slot width b of the wall jet was adjustable within the range of 2 mm $\leqslant b \leqslant$ 8 mm. The jet exit was mounted flush with the test section wall. The slot spanned the whole test section, which had a width $B = 500$ mm.

A thin steel wire was stretched parallel to the wall-jet exit to manipulate the shear layer originating at the nozzle. The diameter of the wire was in the range 0.1 mm $\leqslant D \leqslant$ 0.8 mm. Strain gauges, mounted on the support prongs, enabled the determination of the wire frequency. By varying the tension of the wire the eigenfrequency could be changed. For the case of the still wire, the tension was adjusted as high as possible, limited only by the wire strength. This was necessary to obtain high eigenfrequencies and to avoid the self-excited oscillations. For the case of the oscillating wire, the tension was significantly lowered to obtain eigenfrequencies at $f_w \approx 175$ Hz.

3. The unforced wall-jet

3.1. The shear layer region $0 \leqslant x/b \leqslant 15$

Although the main concern of the manipulation is to alter the wall-jet in the downstream region $x/b > 40$, the actual location of the manipulation is in the immediate vicinity of the wall-jet exit, that is at $x/b \approx 1$.

Schober, Grewe and Fernholz [14] showed in a visualisation study that transition in the present wall jet configuration is driven by shear-layer instability. The shear-layer instability leads to the formation of shear-layer vortices, which undergo several stages of pairing processes and lead to the formation of coherent turbulent structures. The breakdown of these large coherent structures causes the wall jet to become turbulent but even far downstream the flow field is still affected by the upstream shear-layer structures. This behaviour was observed in the Reynolds number range $2500 \leqslant Re_j \leqslant 10000$.

Figure 2(a) shows the evolution of the mean velocity profile of the unforced wall jet in the region close to the nozzle ($0 \leqslant x/b \leqslant 10$). The position $y_{m/2}$ at which the velocity equals half the maximum velocity u_m was subtracted from each profile to eliminate the effect of streamline curvature. The wall jet emerges at $x/b = 0$ with a top-hat velocity profile. For streamwise distances $x/b \leqslant 5$, the shear layer originating at the lip of the wall jet nozzle and the boundary layer near the wall are separated by a potential core.[1] The streamwise

[1] Due to the curvature at the wall jet exit, the hot-wire probe could not be traversed closer than about 1 mm to the wall. Therefore, the boundary layer region is only shown at stations $x/b \geqslant 7$.

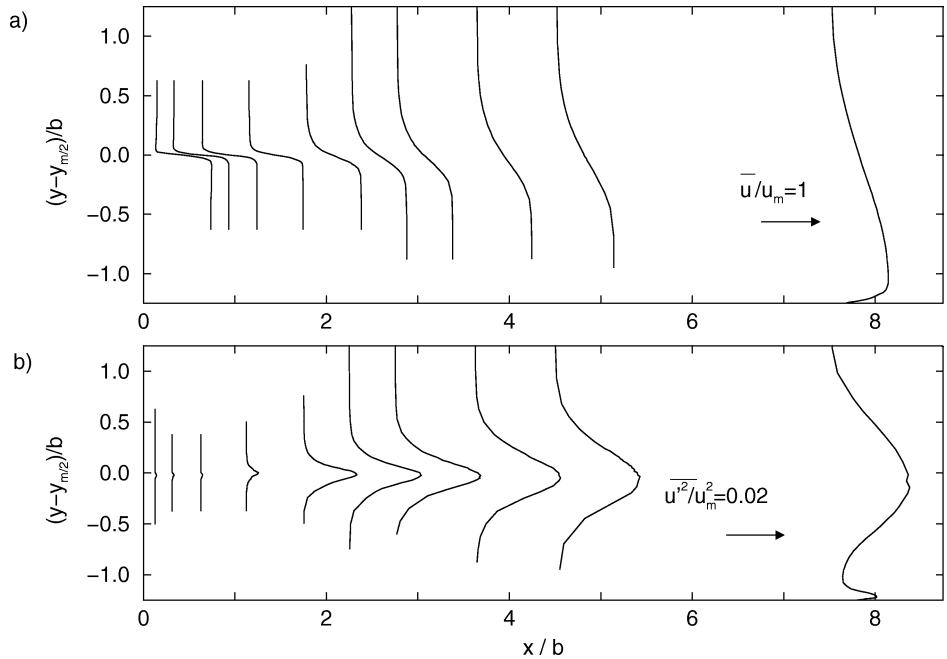

Figure 2. Evolution of the shear layer of the wall jet (unforced); (a) mean velocity, (b) turbulence intensity.

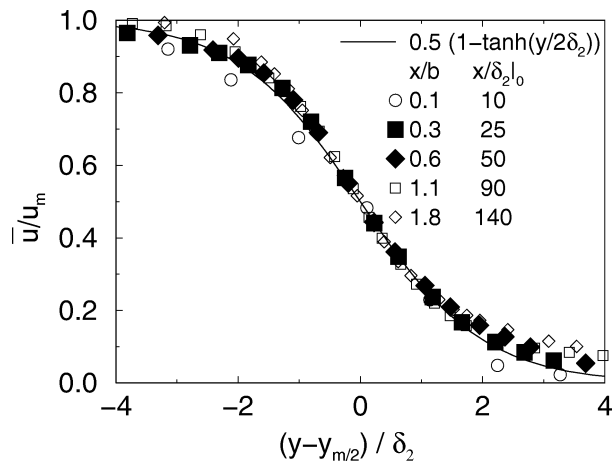

Figure 3. Shear layer profiles (unforced).

turbulence intensity $\overline{u'^2}/u_m^2$, shown in *figure 2(b)*, almost vanishes for $x/b \leqslant 1$ but grows rapidly for $x/b > 1$, indicating the onset of the Kelvin-Helmholtz instability at station $x/b \approx 1$.

The initial shear-layer profiles at the wall-jet nozzle conform closely to the well known tanh-profile of free shear layers (*figure 3*), when normalised with the momentum deficit thickness δ_2. It is therefore not surprising, that the inviscid instability analysis of a tanh-profile (Michalke [15]) explains the shear layer roll-up of the initial stages of the development of the unforced wall-jet. *Figure 4* shows the spectra obtained from hot-wire measurements. The broad peak at $x/b = 1.1$ for $f = 2.9$ kHz corresponds to the initial shear-layer instability and agrees well with the analytical results of Michalke [15]. Further downstream, at $x/b = 1.8$, the occurrence

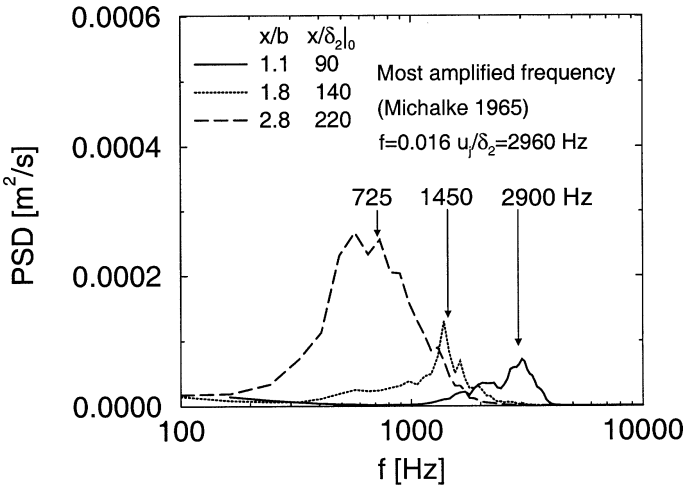

Figure 4. Spectra of the unforced shear layer.

of a subharmonic at $f = 1.45$ kHz indicates the first stage of vortex pairing, and at $x/b = 2.8$ the second subharmonic marks the next stage of pairing.

3.2. The downstream region $25 \leqslant x/b \leqslant 150$

Figure 5 shows profiles of the mean velocity and the turbulence intensity at streamwise distances $40 \leqslant x/b \leqslant 200$. The data is made dimensionless by $y_{m/2}$, the wall distance at which the local velocity is half the maximum velocity u_m. The profiles of the mean velocity show clearly a self-similar behaviour within this region. The mean flow data of Abrahamsson et al. [11] and Eriksson, Karlsson and Persson [16] agree perfectly with

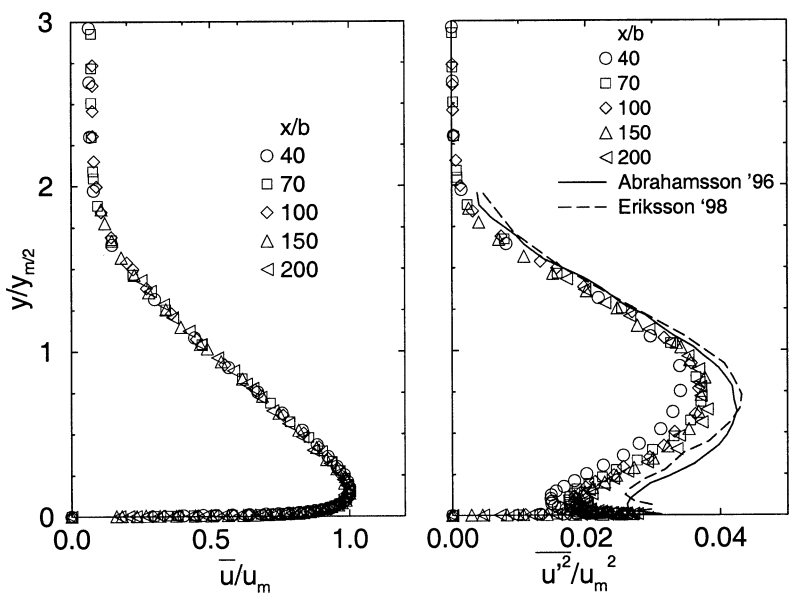

Figure 5. Profiles of the mean velocity and the turbulence intensity (unforced, $b = 4$ mm).

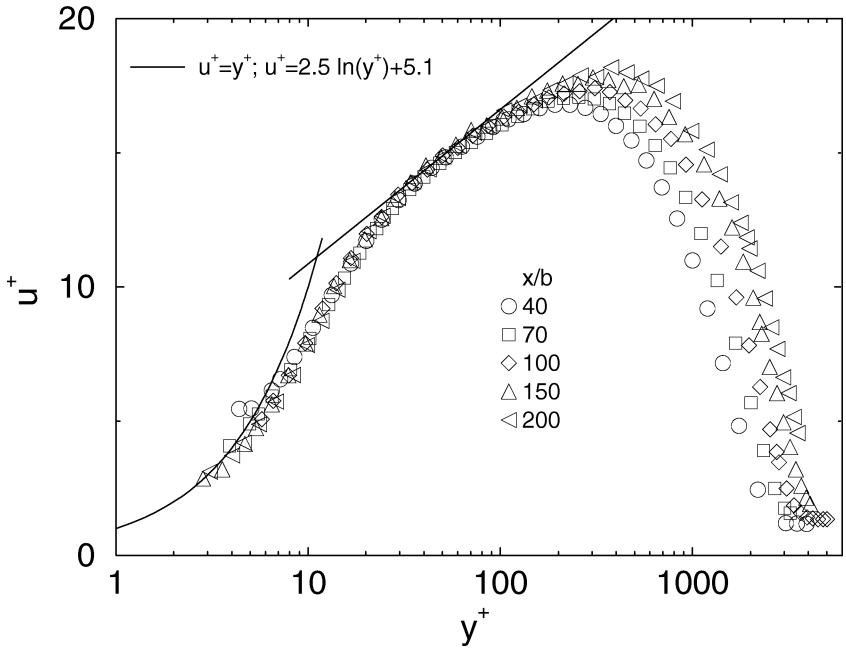

Figure 6. Velocity profiles in inner-law scaling (unforced, $b = 4$ mm).

the present data, so they are not shown. The turbulence intensity $\overline{u'^2}/u_m^2$ shows self-similar behaviour too, but the region is smaller ($70 \leqslant x/b \leqslant 150$). The discrepancies between the present turbulence data and those of Abrahamsson [17] and Eriksson et al. [16] lie in the different boundary conditions at the origin of their wall jet since they used a vertical wall above the wall-jet nozzle.

When normalized with the skin friction velocity u_τ, the velocity profiles reveal a small but distinct logarithmic region within $30 < y^+ < 80$ (*figure 6*).

The development of the turbulence in a wall-jet needs a certain minimum distance from the wall-jet nozzle, e.g. for the mean flow data $x/b \geqslant 25$ is sufficient. Narasimha, Narayan and Parthasarathy [18] showed that the effects of the wind tunnel side walls become important for streamwise distances $x/B > 1.7$, where B is the width of the wind tunnel. The data presented in *figures 5* and *6* was obtained with a slot-width $b = 4$ mm, leading to a maximum value of $x/B = 1.6$.

4. Turbulence suppression by means of a still trip-wire

In this section the manipulation of the shear layer by a small obstacle, a still trip-wire, is described. We first define a measure of the effectiveness and thereafter study the parameters affecting it.

The Reynolds number, based on slot width $b = 8$ mm was $Re_j = 10000$, unless stated otherwise.

4.1. A measure of the effectiveness

As already mentioned in section 1, previous investigations have shown that a small cylinder or wire can significantly reduce the turbulence level in a shear or mixing layer. A general shortcoming was, however, that the parameters governing the mechanism of turbulence reduction, such as wire diameter and its position, have

not been studied in detail. This is probably due to the difficulties involved with quantifying the effectiveness of the manipulation. If, for instance, the spreading rate of a shear layer is chosen to be a measure of the effectiveness, a parametric study of a few relevant parameters would require the measurement of a vast amount of velocity profile data.

In a wall jet, however, most of the changes that disturb the velocity profile are reflected in the value of the skin friction. As the amount of momentum of the wall jet is fixed at the wall-jet nozzle, a reduction of the spreading rate results in an increase of the skin friction. Thus, the change of skin friction relative to the undisturbed case τ_w/τ_{w0} was chosen as a measure of the effectiveness $\mathcal{E}$. The streamwise position at which the wall shear stress was compared was $x/b = 40$.

4.2. Dimensional analysis

The skin friction and hence the effectiveness of the manipulation will depend upon the following parameters:

- the skin friction without forcing τ_{w0};
- the characteristic velocity of the flow around the wire u_D;
- the kinematic viscosity ν;
- the momentum deficit thickness at the nozzle $\delta_2|_0$;
- the diameter D of the wire; and
- its position (x_D, y_D).

$$\tau_w = \mathcal{F}(\tau_{w0}, u_D, \nu, \delta_2|_0, D, x_D, y_D). \tag{1}$$

Other quantities, like the jet exit velocity u_j, the slot width b and the slot length B do not appear in this list, since their effect is accounted for in the value of the unforced skin friction τ_{w0}. Furthermore, these quantities were not varied.

From the above set of relevant quantities we choose (ν, u_D, τ_{w0}) as a natural dimension base. The advantage of having ν/u_D as a characteristic length rather than D is that the diameter is now isolated in the wire Reynolds number $Re_D = Du_D/\nu$. We obtain the following non-dimensional parameters:

$$\mathcal{E} = \frac{\tau_w}{\tau_{w0}} = \mathcal{F}_1\left(\frac{D\,u_D}{\nu}, \frac{\delta_2|_0\,u_D}{\nu}, \frac{x_D\,u_D}{\nu}, \frac{y_D\,u_D}{\nu}\right). \tag{2}$$

The influence of the parameters in equation (2) can be studied best if the position (x_D, y_D) of the wire in the region of the nozzle exit is optimized first. For this purpose the wire was traversed on a rectangular mesh. At each position of the wire the skin friction was measured by means of a Preston tube located at $x/b = 40$. The effectiveness $\mathcal{E} = \overline{\tau}_w/\overline{\tau}_{w0}$ was then calculated and is shown as a contour plot in *figure 7*. The most effective region ranges from $x_D \approx 1$ mm to $x_D \approx 6$ mm along the shear layer. The vertical extent of this region is comparatively small and spans ≈ 0.5 mm. The shape of this most effective region is oriented slightly upward since the wall jet initially emanates in this direction and turns into the horizontal direction due to the Coanda effect.

From *figure 7* two main conclusions can be drawn: (1) the trip wire must be positioned very accurately in the middle of the shear layer; (2) the trip wire must be positioned upstream of the natural shear-layer roll-up. As we will discuss in the next section, the shear-layer instability is suppressed and the wake of the wire causes transition of the wall jet.

Since the wire is most effective in the middle of the shear layer the characteristic flow velocity is $u_D = 0.5u_j$. The resulting Reynolds numbers cover the range $125 < Re_D < 500$ which is above the critical Reynolds number

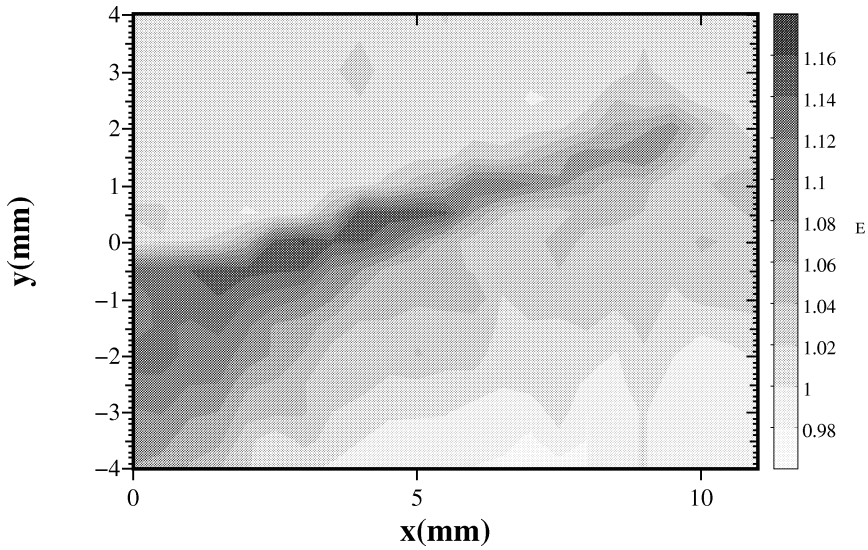

Figure 7. Optimal trip wire position.

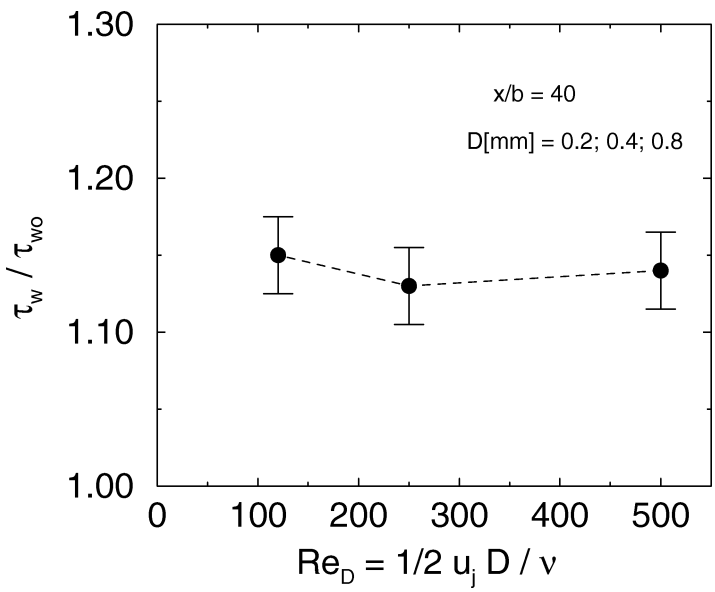

Figure 8. Dependence of the effectiveness τ_w/τ_{w0} on the wire Reynolds number ($Re_j = 10000$; $b = 8$ mm).

of a Kármán vortex street ($Re_D \approx 40$) but still in a range where vortex streets exist (e.g. Tritton [19]). So the effect of the wire is to generate a Kármán vortex street prior to the natural shear-layer roll-up. This vortex street causes transition in the shear layer and prevents the generation of the shear-layer vortices.

For the investigation of the influence of the wire Reynolds number Re_D, the wire diameter D was varied at constant jet velocity u_j and thus constant Reynolds number based on momentum deficit thickness $Re_{\delta 2}$. The position of each wire was optimised for giving the highest effectiveness, which always resulted in a position in the middle of the shear layer. *Figure 8* shows that the wire Reynolds number does practically not affect the

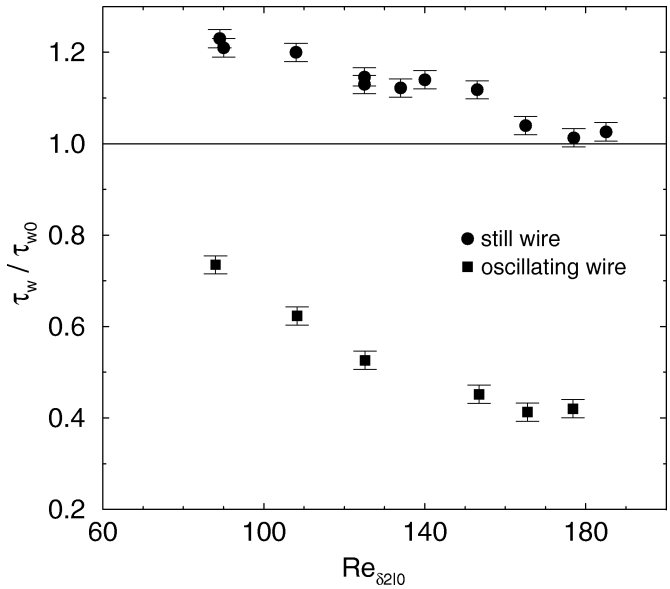

Figure 9. Dependence of the effectiveness τ_w/τ_{w0} on $Re_{\delta_2|_0}$ ($5000 \leqslant Re_j \leqslant 15000$; $b = 8$ mm).

effectiveness in the range investigated here. This result agrees with Tong and Warhaft [7] who found also that a change of the wire Reynolds number did not change the turbulence suppression in their axisymmetric jet.

The influence of the Reynolds number $Re_{\delta 2} = \delta_2|_0 u_D/\nu$ was investigated changing the jet exit velocity. $\delta_2|_0$ is the momentum deficit thickness of the shear layer at the nozzle exit. In order to save space we have included in some figures results obtained for the oscillating wire. These data will be discussed in section 5. *Figure 9* shows that the effectiveness decreases strongly with $Re_{\delta 2}$. This can be explained as follows:

The flow visualisations by Schober et al. [14] have shown that the shear-layer instability leads to the formation of vortices in the unforced wall jet. As a first approximation, we assume that a typical length scale of the vortices is given by $\lambda = u_c/f$ where f is the roll-up frequency and $u_c = 0.5u_j$ the convection velocity of the vortices. The momentum deficit thickness of the emanating laminar shear layer at the nozzle can be approximated by $\delta_2|_0 \propto \sqrt{\nu L/u_j}$ where L is a characteristic length of the nozzle. From the definition of the Strouhal number $St = f\delta_2|_0/u_j$ we find that

$$\lambda \propto \frac{1}{St}\sqrt{\frac{\nu L}{u_j}} = \frac{\sqrt{bL}}{St}\frac{1}{\sqrt{Re_j}}. \tag{3}$$

Thus, the typical length scale λ of the (unforced) shear layer vortices decreases with $Re_j^{-1/2}$. As will be shown in the next section, the trip wire basically introduces small structures. Since the natural shear layer vortices become smaller with increasing Reynolds number, the wire is less effective.

4.3. The shear layer region $0 \leqslant x/b \leqslant 15$

Figure 10(a) compares the evolution of the velocity profiles of the unforced and the tripped wall jet in the region close to the nozzle ($0 \leqslant x/b \leqslant 10$). Although the profiles for the two cases were not taken at identical streamwise positions a comparison is possible. The wake of the trip wire is clearly noticeable in the first profile ($x/b = 0.44$) but decays very rapidly, so that no trace is left in the next profile at $x/b = 0.625$.

The trip wire causes an increase of the streamwise turbulence intensity $\overline{u'^2}/u_m^2$ immediately behind the wire, as shown in *figure 10(b)*. The turbulence level introduced by the wire grows rather slowly with increasing streamwise distance, whereas turbulence intensity generated by the shear-layer roll-up of the unforced case increases much faster. Therefore, the turbulence intensity of the tripped shear layer is smaller than of the unforced case, downstream of the initial region ($x/b > 2$).

The effect of the suppression of turbulence can also be seen clearly in the development of the shear-layer momentum-deficit thickness δ_2, which is plotted in *figure 11*. For the unforced case, the momentum deficit thickness remains almost constant for $x/b < 1$ but grows rapidly thereafter. The trip wire initially thickens the

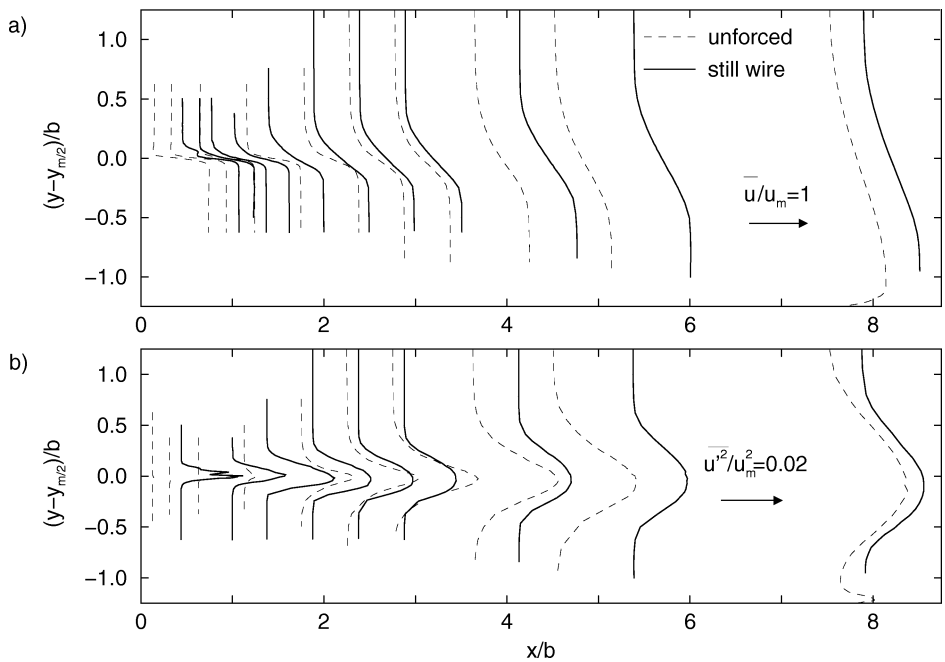

Figure 10. Development of the shear layer of the wall jet (still wire); (a) Mean velocity, (b) Turbulence intensity.

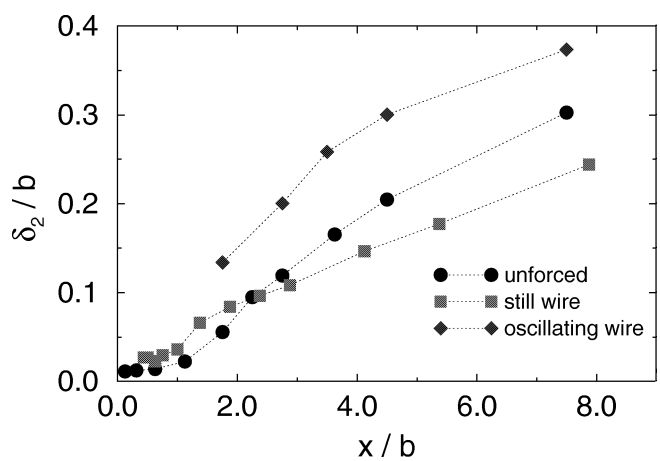

Figure 11. Momentum deficit thickness of shear layer as a function of streamwise location for the unforced case and for the still and oscillating wire.

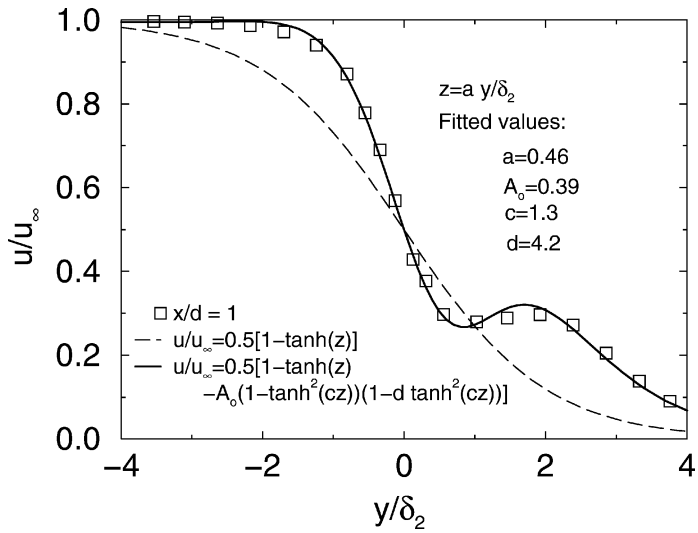

Figure 12. Shear layer profiles (with and without trip wire).

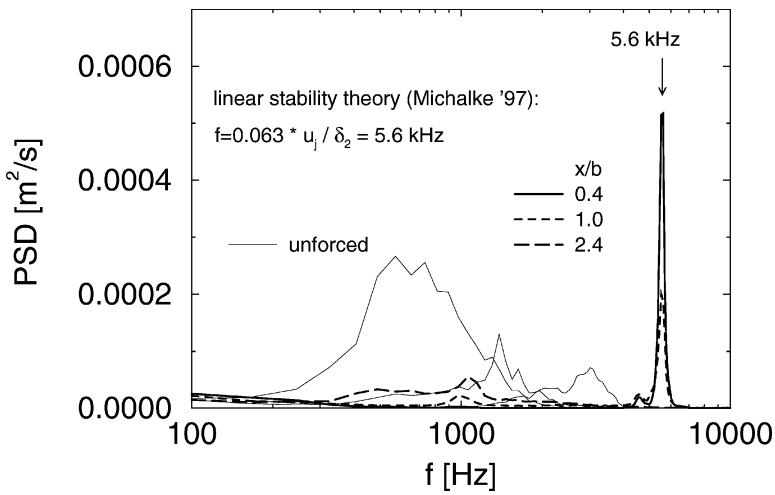

Figure 13. Spectra of the tripped shear layer.

shear layer, but also causes a smaller growth rate, such that for $x/b \geqslant 2$ the tripped shear layer is thinner than the unforced shear layer.

The wake of the wire significantly changes the shape of the *tanh* profile observed without forcing (*figure 12*). So the *tanh* profile had to be modified and is approximated by

$$\frac{u(y)}{u_m} = 0.5\left[1 - \tanh(z) - A_0\left(1 - \tanh^2(cz)\right)\left(1 - d\tanh^2(cz)\right)\right] \tag{4}$$

with the additional parameters (A_0, c, d) accounting for the depth, the width and the overshoot of the wake. Despite the fact that the wake of a cylinder represents an absolutely unstable flow (Koch [20], Monkewitz [21]), a linear spatial stability analysis by Michalke [22] based on the modified velocity profile was able to predict the frequency of the structures behind the wake.

In *figure 13* the spectra behind the wire are compared with those of the unforced case. At $x/b = 0.4$, a sharp peak at $f \approx 5.6$ kHz marks the structures introduced by the trip wire. This peak is in good agreement with the Strouhal number $St = f\delta_2/u_j = 0.063$ obtained by the linear stability analysis. Further downstream, at $x/b = 1.0$, this peak is significantly reduced. It should be noted that there are no signs of subharmonics which indicates the suppression of the vortex pairing process. A similar behaviour is observed in the von Kármán vortex street, where pairing is also inhibited.

4.4. The downstream region $25 \leqslant x/b \leqslant 100$

So far we have used the increase of skin friction at a fixed position $x/b = 40$ as a measure of the effectiveness of the trip wire. *Figure 14* compares the streamwise distribution of the surface shear stress with and without the trip wire. The wire enhances the friction in the entire region ($20 < x/b < 120$) although the effect is stronger close to the nozzle.

The trip wire does not influence the two-dimensionality of the flow. *Figure 15* shows the skin-friction distribution in spanwise direction. For a better comparison, the friction is normalised by $c_f(z/B = 0)$. The friction distribution with and without trip wire is uniform to within $\pm 4\%$.

The trip wire has little effect on the self-similarity of the mean velocity profiles shown in *figure 16*, but affects significantly the turbulence profiles of $\overline{u'^2}/u_m^2$. With increasing streamwise distance the unforced and the tripped Reynolds stress profiles approach each other, but it is not until $x/b = 70$ that the profiles achieve the self-similar shape of the unforced case.

When plotted in wall coordinates, the profiles of the mean velocity (*figure 17*) reveal a small but distinct logarithmic region for $30 \leqslant y^+ \leqslant 100$. The extent of this region increases slightly with increasing streamwise distance. Since $Re_{\delta 2}$ increases for the downstream profiles, the growth of the log-law range can be compared with the behaviour of a zero pressure gradient boundary layer (Fernholz and Finley [23]).

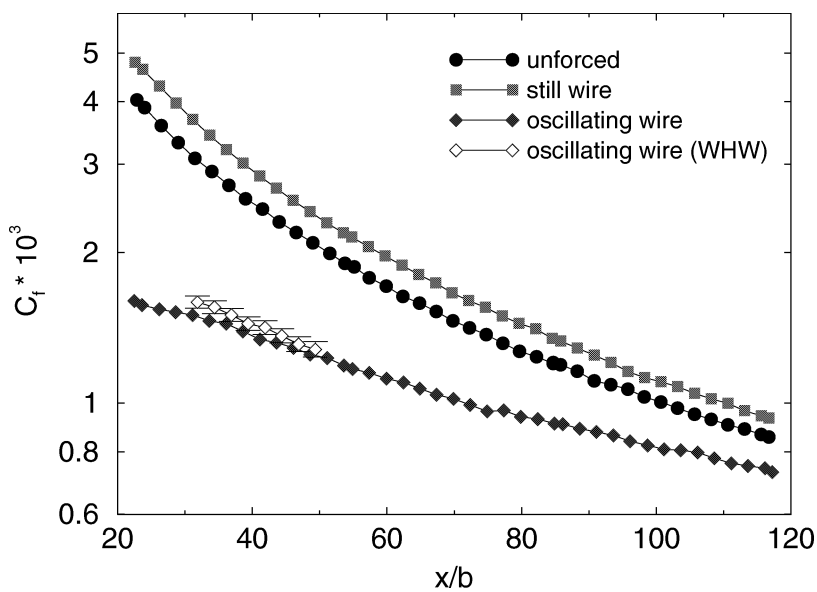

Figure 14. Effect of the manipulations on the skin friction distribution in streamwise direction.

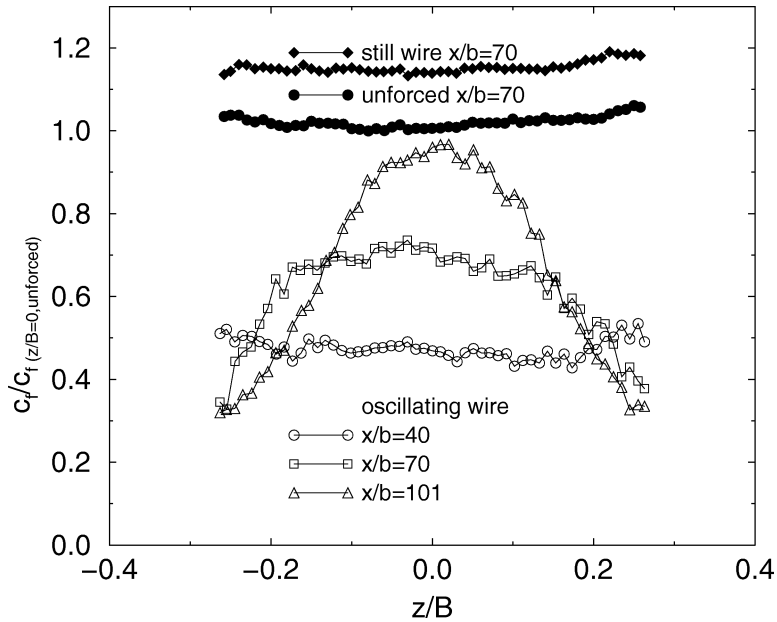

Figure 15. Spanwise skin friction distribution for the three cases: unforced, with still wire and with oscillating wire.

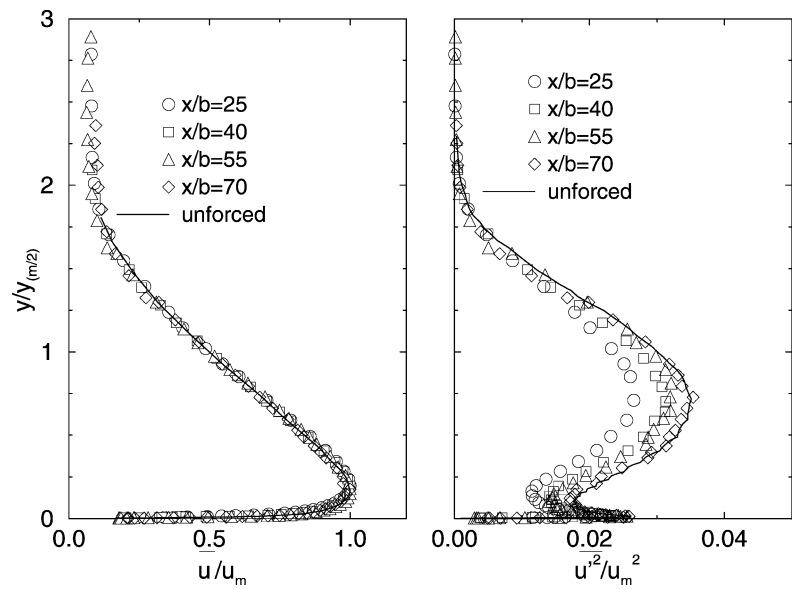

Figure 16. Profiles of the mean velocity and the turbulence intensity (still wire).

5. Turbulence enhancement by means of an oscillating wire

During the investigation of the still wire the wire started to perform flow-induced oscillations, provided that it was located in the shear layer and that the tension of the wire was sufficiently low. The path of the wire resembles a circle (see *figure 1*). The wire is oscillating with its eigenfrequency, which can be adjusted by changing the tension of the wire. A similar phenomenom was reported by Vandsburger and Ding [10], who

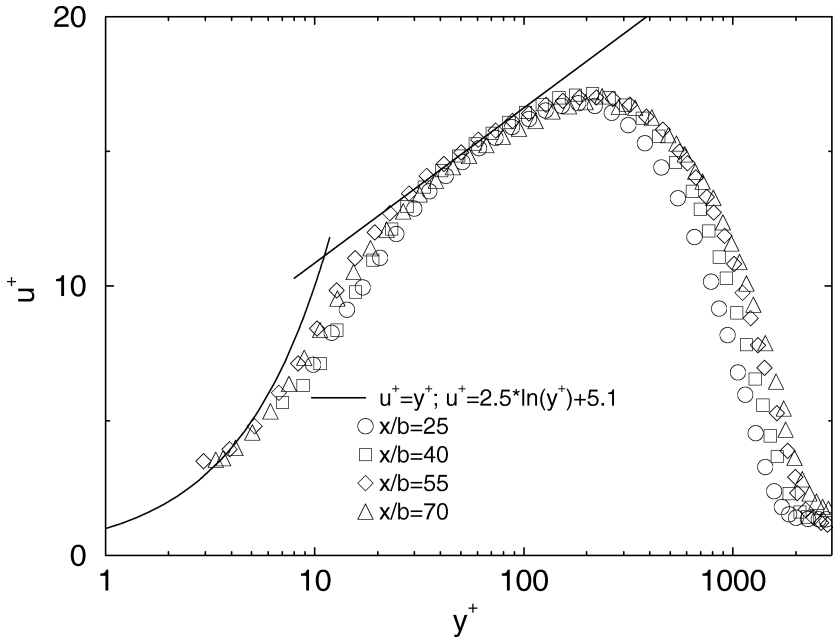

Figure 17. Velocity profiles in inner-law scaling (still wire).

called it 'music wire'. The driving mechanism behind this flow induced oscillation is interesting in itself, and an explanation of this phenomenon is attempted in appendix A.

5.1. Dimensional analysis

In addition to the discussion in section 4.2, the following quantities have to be taken into account for the dimensional analysis when the wire performs oscillations:

- the amplitude of the oscillation A;
- the (eigen)frequency of the wire f_D.

Again, with (ν, u_D, τ_{w0}) as a natural dimension base we arrive at

$$\frac{\tau_w}{\tau_{w0}} = \mathcal{F}_1\left(\frac{D\,u_D}{\nu}, \frac{\delta_2|_0\,u_D}{\nu}, \frac{x_D\,u_D}{\nu}, \frac{y_D\,u_D}{\nu}, \underbrace{\frac{A\,u_D}{\nu}, \frac{f_D\,\nu}{u_D^2}}_{\text{new}}\right). \tag{5}$$

For the investigation of the influence of the parameters in equation (5) we follow a similar pattern as for the still wire in section 4 but we remind the reader that now the goal is to obtain values of the effectiveness which are smaller than one. The location of the oscillating wire is determined by the effectiveness of the oscillation on the flow and by the amplitude of the wire movement. The position of the wire x_D in streamwise direction was chosen as 6.5 mm downstream of the nozzle exit to allow for relatively large amplitudes. The distance normal to the wall was varied in the range 7.2 mm $\leqslant y_D \leqslant$ 8.6 mm. In this range the effectiveness is approximately constant with a value of about 0.51 (*figure18*). The dimensions chosen here limit peak to peak amplitudes to about 12 mm in order to avoid collisions of the wire with the lip of the nozzle.

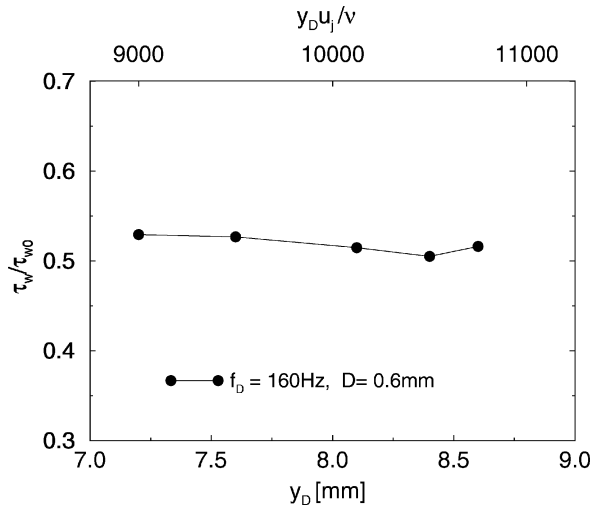

Figure 18. Dependence of the effectiveness τ_w/τ_{w0} on the normal position of the oscillating wire.

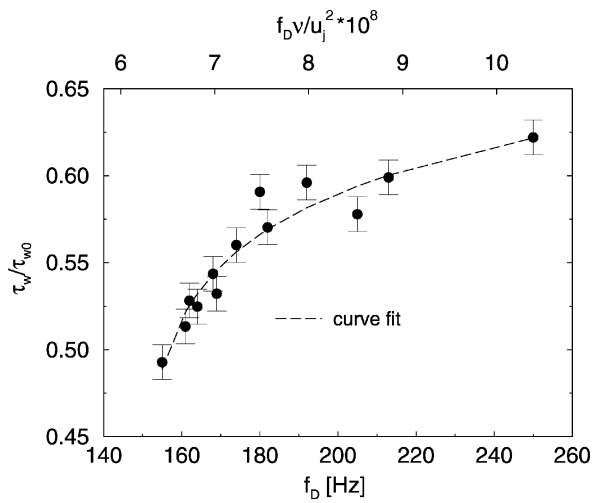

Figure 19. Dependence of the effectiveness τ_w/τ_{w0} on the wire frequency.

It should be noted, however, that only within a narrow region around the middle of the shear layer the oscillation will start without an additional initial excitation. If the wire is positioned outside this region, the oscillation has to be initiated manually.

Since the wire performs a self-excited oscillation it oscillates with its eigenfrequency and the frequency and amplitude cannot be varied independently of each other. A low eigenfrequency causes a large amplitude and vice versa. The eigenfrequency can, however, be changed by adjusting the tension of the wire. *Figure 19* shows that low frequencies (which correspond to large amplitudes) have the strongest effects on the effectiveness. The dimensionless frequency (see equation (5)) is given on top of the figure.

For the investigation of the influence of the wire Reynolds number Re_D three wire diameters and two exit velocities were used. *Figure 20* shows that the effectiveness is practically independent of Re_D if the exit velocity or the jet Reynolds number Re_j is kept constant.

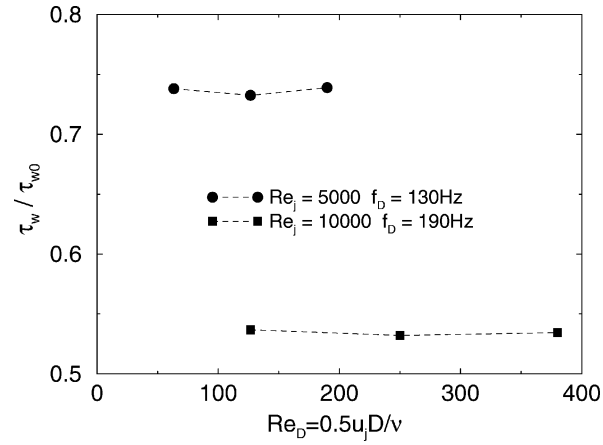

Figure 20. Dependence of the effectiveness τ_w/τ_{w0} on the wire Reynolds number ($D = 0.2$; 0.4; 0.6 mm) and the jet exit velocity.

$Re_{\delta 2}$ was varied by changing the jet exit velocity u_j. For the oscillating wire the effectiveness $\mathcal{E}$ tends to smaller values with increasing Reynolds number $Re_{\delta 2}$ (*figure 9*). Flow visualisation pictures showed (Schober et al. [14]) that the wire generates large scale vortical structures. The size of these structures does not depend on the shear layer properties but rather on the oscillation frequency. Since the size of the natural shear layer structures decreases with increasing Reynolds number, the ratio of the size of the forced structures to the natural structures becomes larger. This leads to an increased effectiveness – here smaller values of τ_w – at large Reynolds numbers.

5.2. The shear layer region $0 \leqslant x/b \leqslant 15$

Figure 21 shows the evolution of the mean velocity and turbulence profiles close to the nozzle. The path of the oscillating wire and the profiles of the undisturbed case are included for comparison. The oscillating wire causes a much shallower velocity distribution and the gradient $\mathrm{d}u/\mathrm{d}y$ is generally smaller than in the unforced case. The maxima of the turbulence intensity $\overline{u'^2}/u_m^2$ are about twice as large since the oscillating wire increases the turbulent kinetic energy and wider than in the unforced case. The momentum deficit thickness is also larger than in the other two cases (*figure 11*).

For a qualitative comparison of the measured data with the flow visualisation movies of Schober et al. [14], phase locked X-wire measurements have been performed. The phase angle of the oscillating wire was determined by the signal of the strain gauge described in section 2. The vorticity was approximated by

$$\Omega_z \approx -\frac{\partial u}{\partial y}$$

and is shown in *figure 22*. The (dark) regions of high vorticity compare well with the vortical structures of the flow visualisations.

Figure 23 compares the spectra downstream of the oscillating wire with those of the unforced case. At $x/b = 1.75$, a sharp peak at $f \approx 340$ Hz marks the first harmonic of the wire frequency. As described by Schober [14], the wire generates one vortex on each pass through the shear layer. Since for each revolution the wire passes the shear layer two times, two vortices are generated per cycle. These vortices undergo the first stage of vortex pairing very rapidly, such that at $x/b = 3.5$ the first harmonic decreases and the fundamental increases. This trend continues at larger streamwise distances $x/b = 7.5$. Please note the different axes for

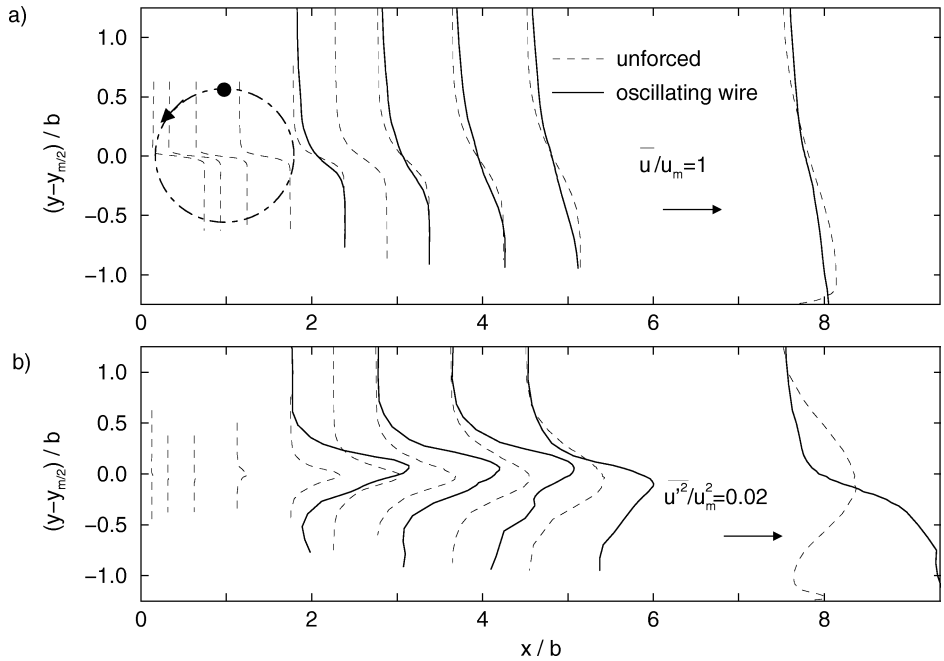

Figure 21. Development of the shear layer of the wall jet (oscillating wire); (a) Mean velocity, (b) Turbulence intensity.

the oscillating and the unforced spectra, which become necessary since the energy contained in the structures introduced by the oscillating wire is roughly three orders of magnitude higher than the energy contained in the shear-layer structures of the unforced case.

From the increase of the turbulent kinetic energy it can be anticipated that the wire will strongly increase the production of the turbulent kinetic energy in the shear layer near the wall jet nozzle. Measurements of all the terms of the turbulent kinetic energy balance have not been attempted, but *figure 24* shows the production term

$$P_{uu} = \overline{u'v'}\,\frac{\mathrm{d}u}{\mathrm{d}y}\,\frac{b}{u_m^3},$$

along the streamwise distance for the three cases and *figure 25* the overall production within the shear layer

$$\int_{\delta} P_{uu}\,\mathrm{d}\left(\frac{y - y_{m/2}}{b}\right).$$

For the unforced case (*figure 24(a)*), P_{uu} remains almost zero for $x/b \leqslant 1.1$, but grows rapidly thereafter due to the shear-layer roll-up. For $x/b \geqslant 2.75$ the peak value decreases but broadens, such that the overall production within the shear layer decreases rather slowly (*figure 25*) with increasing streamwise distance. The presence of the still wire, namely the non-symmetric wake, causes the production to become negative immediately behind the wire at $x/b = 0.7$ (*figure 24(b)*), but already at $x/b = 1.1$ the production is positive and approximately twice as large as in the unforced case. Again, with increasing streamwise distance the peak value decreases and broadens, such that the overall production shown in *figure 25* decreases slowly for $x/b \geqslant 1.75$. For $x/b \geqslant 4$, the overall production in the disturbed shear layer is smaller than in the unforced case. The oscillating wire causes a strong increase in turbulence production compared with the other two cases.

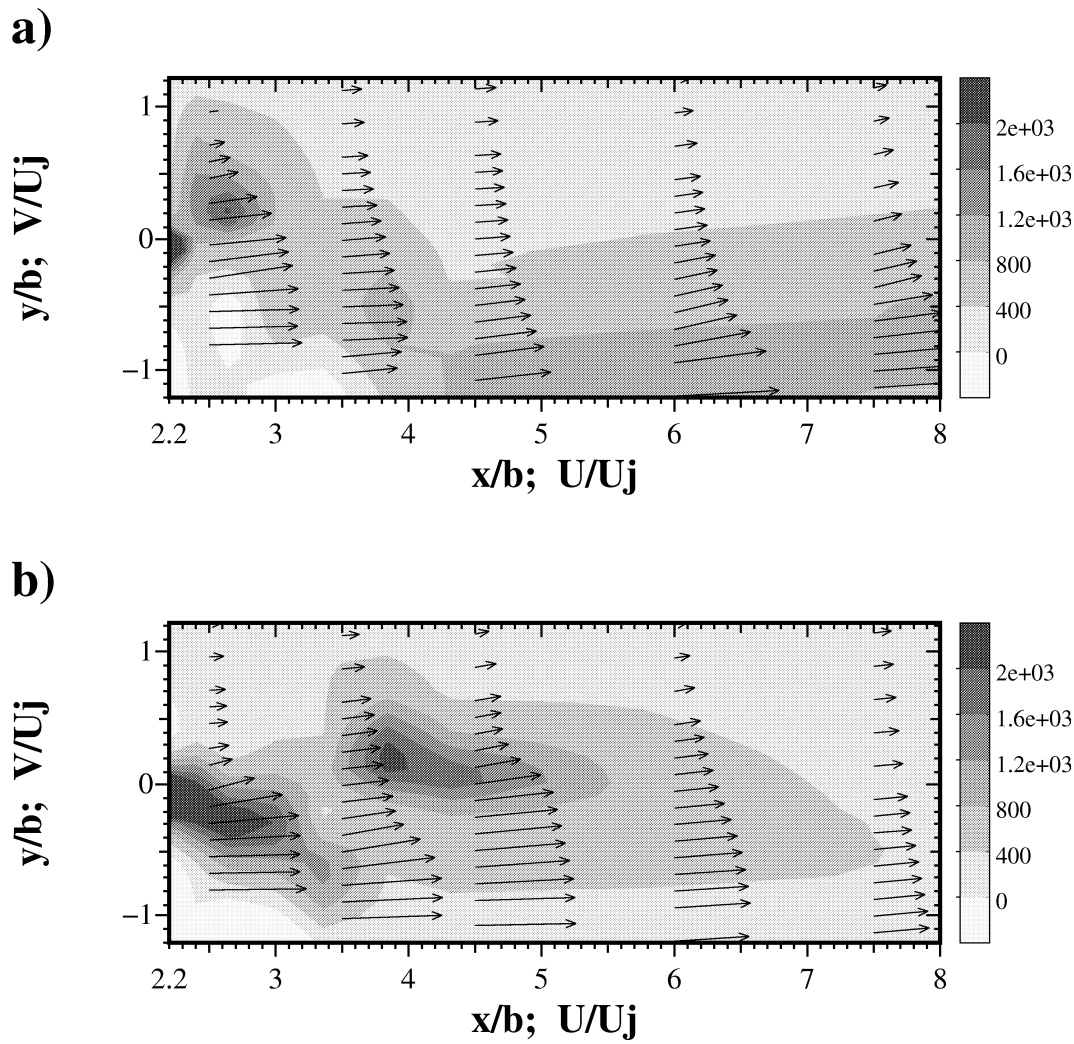

Figure 22. Velocity vectors and vorticity in the shear layer at different phase angles of the wire: (a) 30°; (b) 210°.

The peak in *figure 24(c)* is larger and broader than previously and the overall production shown in *figure 25* is nearly twice as large as for the tripped case.

5.3. The downstream region $25 \leqslant x/b \leqslant 100$

The skin friction at $x/b = 40$ has already been used as an indicator of the effectiveness of the manipulation. *Figure 14* compares the skin-friction distribution in the streamwise direction for the unforced wall jet and the wall jet manipulated by a still and an oscillating wire, respectively. The oscillating wire reduces the wall shear stress in the region $20 < x/b < 120$, but the effect is more pronounced close to the nozzle and decreases with streamwise distance.

In order to gain further insight into the turbulence structure near the wall, we measured the turbulence intensity $Tu = \sqrt{\overline{c_f'^2}/\overline{c_f}} * 100$ of the skin friction (*figure 26*) and the probability density functions for the three cases (*figure 27*). The turbulence intensity of the unforced wall jet appears to rise slowly from 32% at

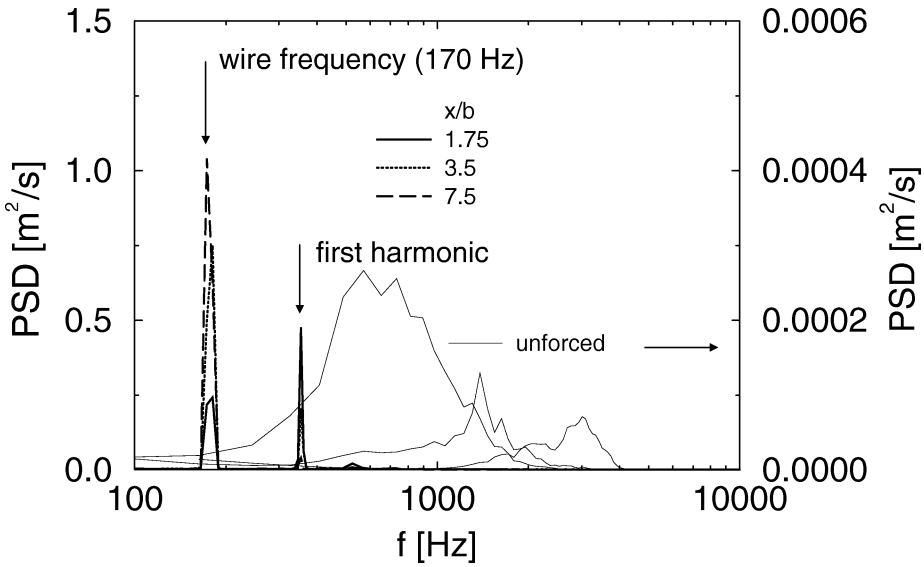

Figure 23. Spectra of the shear layer with and without the oscillating wire at three streamwise locations.

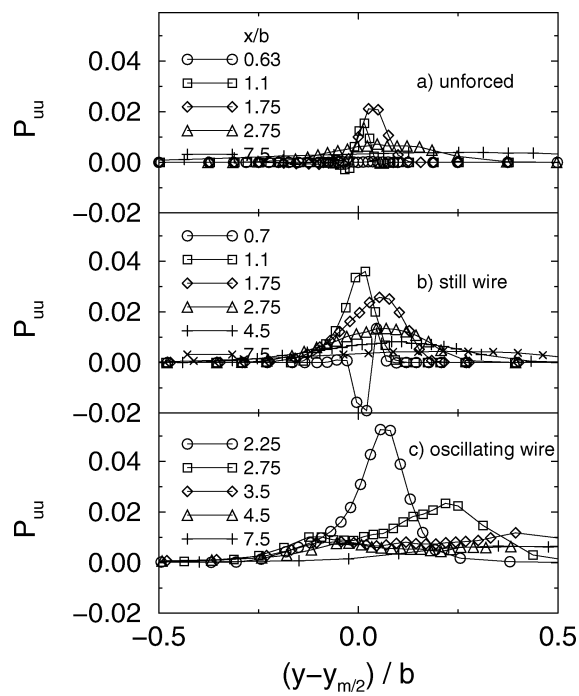

Figure 24. Production term P_{uu} for the unforced wall jet, the still wire and the oscillating wire.

$x/b = 25$ to 38% at $x/b = 55$. The measurements are probably too low, however, because of the large active length of the hot wire. The active length of a hot wire should not exceed $l^+ = 20$, where l^+ is the viscous length $u_\tau l/\nu$ (Johansson and Alfredsson [24]). For $x/b < 55$ this value is exceeded and thus the value of the turbulence intensity is measured too low. The turbulence intensity of the flow manipulated by the still wire is not changed compared with that of the unforced case. However, the oscillating wire causes a dramatic increase

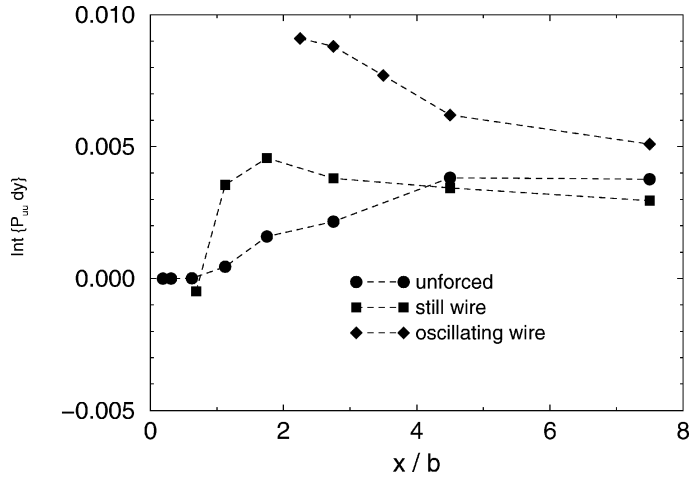

Figure 25. Overall production in the shear layer for the three cases.

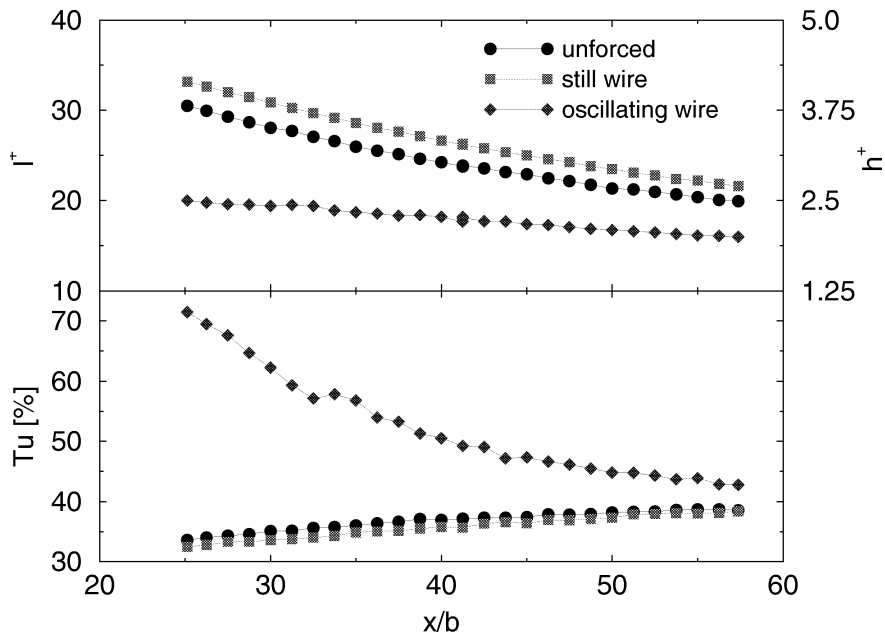

Figure 26. Turbulence intensity of the skin friction and $l+$ (wall hot wire).

of the turbulence intensity of the skin friction. The value of 70% at $x/b = 24$ is nearly twice as large as for the unforced case.

The PDFs of the unforced wall jet are independent of the streamwise position (*figure 27*). The PDFs are not symmetrical but are skewed so that the skewness is positive. This is characteristic of zero-pressure-gradient boundary layers. The instantaneous velocities range from 0.25 to 3.5 times the mean velocity. The presence of the still wire has no noticable effect on the shape of the PDFs. However, the oscillating wire changes the shape of the PDFs considerably. The skewness is much more pronounced at $x/b = 25$, where the instantaneous velocity reaches six times the mean velocity. With the decrease of the disturbance in streamwise direction the PDF returns slowly to the PDF of the unforced case.

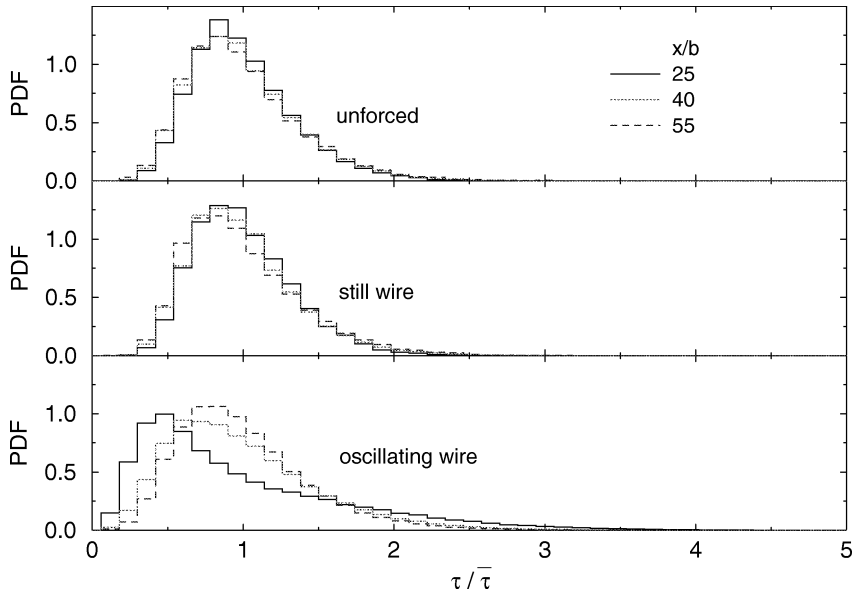

Figure 27. Probability-density-function of the skin friction (wall hot wire).

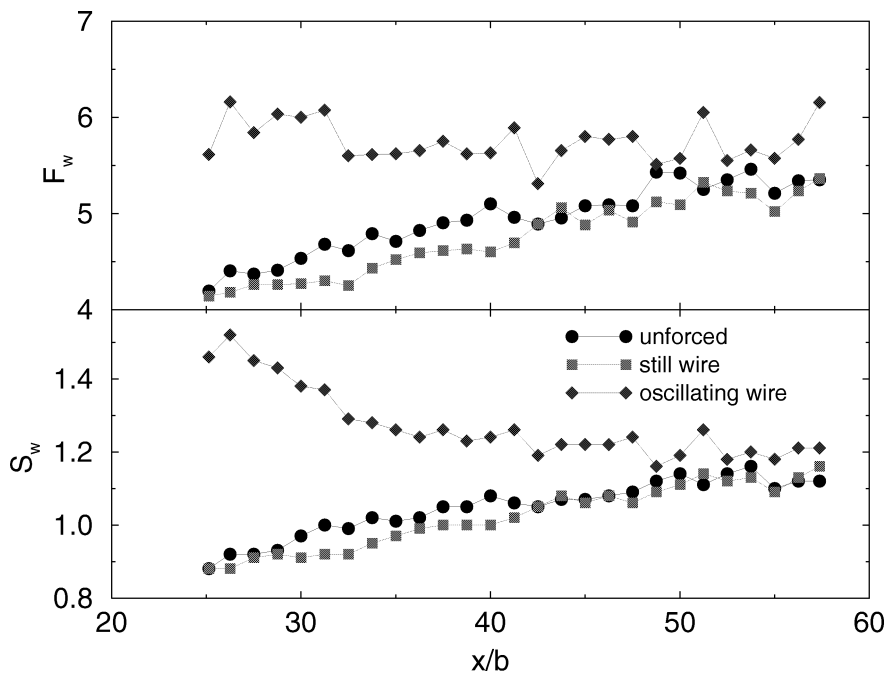

Figure 28. Skewness (S_w) and flatness (F_w) of the skin friction (wall hot wire).

Figure 28 presents the skewness S_w and the flatness F_w as a function of the streamwise position for the three cases. Again the curves for the unforced case and the still wire are very close to each other. The curves for the oscillating wire clearly deviate from the unforced case, underlining the severe changes of the turbulence structure in the near wall region of the wall jet.

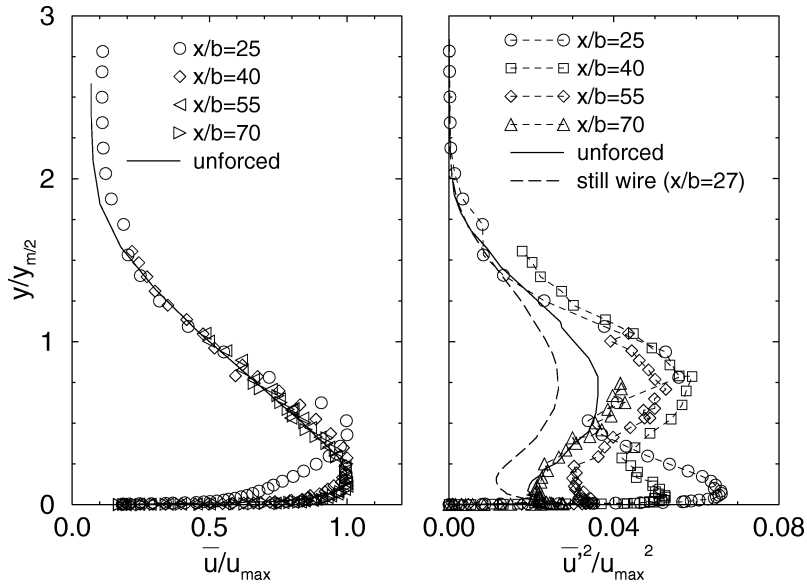

Figure 29. Profiles of the mean velocity and the turbulence intensity (oscillating wire).

Since the amplitude of the oscillation of the wire varies along the span – it is zero at the support prongs and largest at the centerline of the test section, – the two-dimensional behaviour of the unforced wall jet will become three-dimensional. This may be seen from the spanwise distribution of the skin friction, which becomes three dimensional with increasing streamwise distance (*figure 15*).

The profiles of the mean velocity and the turbulence intensity of the wall jet when manipulated by the oscillating wire are shown in *figure 29*. The mean velocity profile at $x/b = 25$ deviates significantly from the self-similar shape of the unforced case. The differences decrease rather rapidly with increasing streamwise distance, so that at $x/b = 55$ the manipulated profile can hardly be distinguished from the unforced one. It should be kept in mind, however, that the scaling is local, the half width $y_{m/2}$ is significantly larger and the local velocity maximum u_m is significantly lower than for the unforced case. The profiles of the turbulence intensity

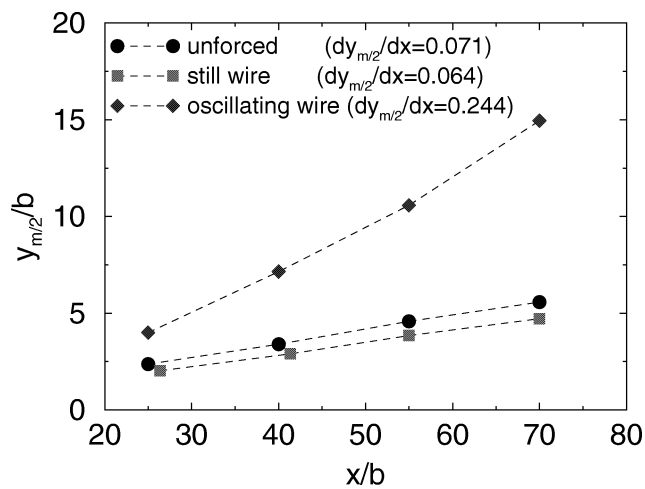

Figure 30. Development of the half-width $y_{m/2}$ in streamwise direction for the three cases.

$\overline{u'^2}/u_m^2$ deviate strongly from the unforced case and do not reach the self-similar form. Close to the nozzle the strong disturbance caused by the oscillating wire and, further downstream, the growing three-dimensionalities prevent the wall jet to reach equilibrium.

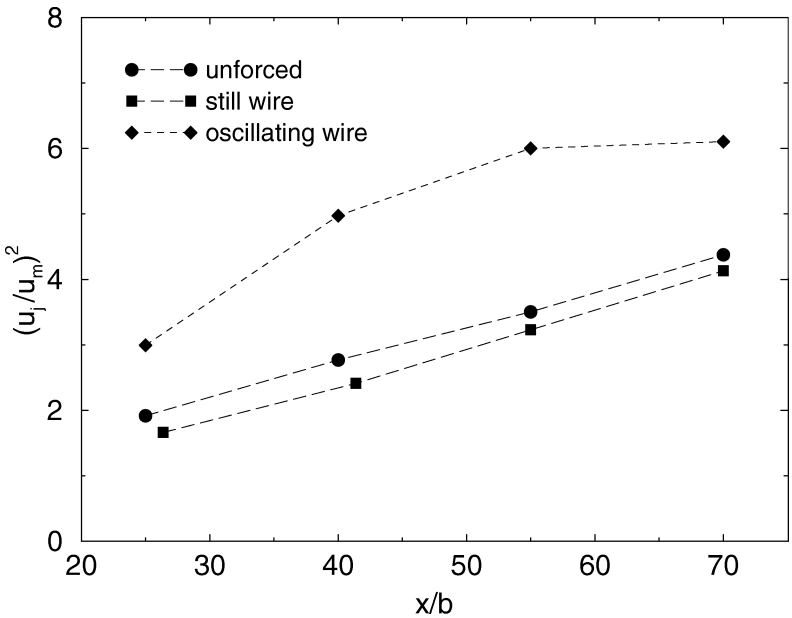

Figure 31. Development of the local velocity maximum in streamwise direction for the three cases.

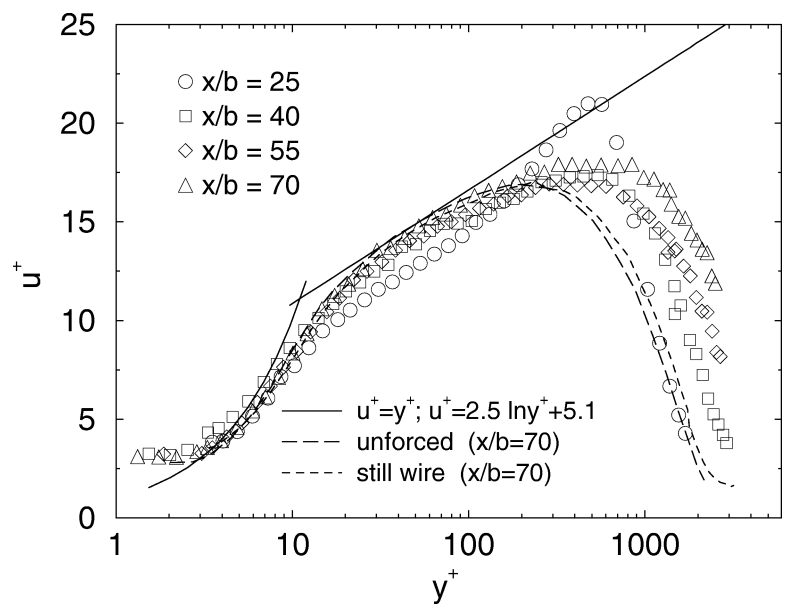

Figure 32. Velocity profiles in inner-law scaling (oscillating wire).

The enhanced mixing results in a faster growth of the momentum deficit thickness in the shear-layer region. In the wall-jet region, the characteristic measure is the evolution of the half width $y_{m/2}$, which is compared for the three cases in *figure 30*. The still wire reduces the growth of the wall jet whereas the oscillating wire enhances its growth. A change in the width will result in a change of the magnitude of the local velocity maximum. The development of the local velocity maximum in streamwise direction is plotted as $(u_j/u_m)^2$ in *figure 31*, since in this scaling the decay of u_m appears to show a nearly linear increase of $(u_j/u_m)^2$ (Launder and Rodi [25]). The still wire causes a higher local velocity maximum u_m compared with the unforced case. The oscillating wire dramatically lowers u_m. Also, the linearity of $(u_j/u_m)^2$ is lost due to the three-dimensionality.

The velocity profiles in inner-law scaling are shown in *figure 32*. The manipulated profiles tend towards the unforced profile with increasing streamwise distance but clearly reveal the influence of the oscillating wire on the near-wall layer close to the nozzle.

6. Conclusions

It has been shown that the present two-dimensional turbulent wall jet leaves the wall-jet nozzle in a laminar state. The Kelvin-Helmholtz instability leads to the formation of shear-layer vortices. These vortices undergo several stages of pairing processes leading to relatively large-scale turbulent structures. The breakup of these shear-layer structures causes transition in the wall jet. Measurements of the mean and fluctuating velocities in the downstream region $25 \leqslant x/b \leqslant 150$ are in good agreement with the recent studies of Abrahamsson et al. [11] and Eriksson et al. [16] of turbulence structure in a wall jet.

The structure of the turbulence in the wall jet can be significantly modified by perturbing the initial shear layer near the nozzle. A thin wire, placed directly behind the nozzle into the shear layer prevents the shear-layer roll-up and pairing processes are no longer observed. The wire significantly reduces the size of the turbulent structures. The spreading of the wall jet and the mixing with the ambient fluid is reduced. The skin friction is increased. The wire has little effect on self-similarity with respect to the mean velocity but a larger effect on the fluctuating velocity. The two-dimensionality of the wall jet is not affected.

A self-excited oscillating wire introduces structures into the initial shear layer which do not depend upon the shear-layer properties but on the wire frequency. Choosing low oscillation frequencies leads to the formation of large vortices, which increase in size over several stages of vortex pairing. This causes a dramatic increase of the spreading rate and the mixing. The skin friction in the wall jet is significantly reduced. The two-dimensionality of the flow is lost due to the three-dimensional nature of the oscillation.

Appendix A. Galloping of a cylinder in simple shear

So far, we have only discussed the influence of the oscillating wire on the flow field but not the reason why the wire actually starts performing flow-induced oscillations.

There are two basic sources for a flow-induced vibration: (1) a vortex-induced vibration, driven by the von Kármán vortex street; (2) a galloping phenomenom.

Since the frequency of the von Kármán vortex street is roughly 30 times the eigenfrequency of the oscillating wire, a resonance can be ruled out. It is thus very unlikely that a vortex-induced vibration generates the large amplitudes observed experimentally. Therefore a model for the galloping of a cylinder in a shear flow is suggested, since the classical galloping model of a body in uniform flow (Blevins [26]) cannot explain the oscillation of a circular cylinder.

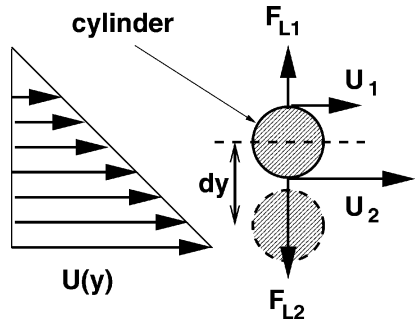

Figure 33. Model for the galloping of a circular cylinder in a linear shear layer.

Figure 33 shows a sketch of a cylinder in a shear layer with a linear velocity profile $U(y)$. The cylinder is split in two halves, a lower and an upper half. The velocity at the edge of each half cylinder is denoted U_1 and U_2. We now estimate the lift force F_{L1} of the upper half-cylinder,

$$F_{L1} = \frac{1}{2}\rho\zeta_A u_1^2, \tag{6}$$

where ζ_A is the lift coefficient of a half-cylinder. Similarly, we obtain for the lower part

$$F_{L2} = \frac{1}{2}\rho\zeta_A u_2^2. \tag{7}$$

The resulting net force F_{net} can be calculated by subtracting the two forces. We obtain

$$F_{net} = F_{L1} - F_{L2} = \frac{1}{2}\rho\zeta_A\left(u_1^2 - u_2^2\right) = \frac{1}{2}\rho\zeta_A \underbrace{(u_1 - u_2)}_{(1)}\underbrace{(u_1 + u_2)}_{(2)}. \tag{8}$$

If the cylinder is now moved a length Δy away from its position at rest, the two velocities u_1 and u_2 will change. In a linear velocity profile, the term (1) will remain constant, but term (2) will change. Therefore, the resulting net force will change as well.

If the cylinder moves into the region of higher velocity, term (2) becomes larger and thus the resulting net-force increases. If the deflection is large enough, the elastic force of the wire will cause a reversal of the motion. When the cylinder moves into the direction of lower velocity, term (2) becomes smaller and the net force will decrease. In both cases the change of net force is in the same direction as the motion, the oscillation is thus excited.

The drag force depends on the velocity and thus on the transverse position of the wire. This force will oscillate as well and deflect the wire in the streamwise direction, which causes the nearly circular path of the wire.

Since the shear layer is thin compared to the oscillation amplitude, the wire periodically leaves and reenters the shear layer. While the wire is outside the shear layer, the lift force described above is not present. A detailed analysis of the equations of motion for the oscillating wire is therefore not trivial due to the complicated forcing.

Acknowledgements

The authors gratefully acknowledge the financial support by the Deutsche Forschungsgemeinschaft (DFG) and the aid of F. Grewe.

References

[1] Freymuth P., On transition in a separated laminar boundary layer, J. Fluid Mech. 25 (1966) 683–704.
[2] Fiedler H.E., Mensing P., The plane turbulent shear layer with periodic excitation, J. Fluid Mech. 150 (1983) 281–309.
[3] Ho C.-M., Huang L.-S., Subharmonics and vortex merging in mixing layers, J. Fluid Mech. 119 (1982) 443–473.
[4] Katz Y., Horev E., Wygnanski I., The forced turbulent wall jet, J. Fluid Mech. 242 (1992) 577–609.
[5] Zhou M.D., Heine C., Wygnanski I., The effects of excitation on the coherent and random motion in a plane wall jet, J. Fluid Mech. 310 (1996) 1–37.
[6] Strykowski P.J., Sreenivasan K.R., On the formation and suppression of vortex 'shedding' at low Reynolds numbers, J. Fluid Mech. 218 (1990) 71–107.
[7] Tong C., Warhaft Z., Turbulence suppression in a jet by means of a fine ring, Phys. Fluids 6 (1) (1994) 328–334.
[8] Rajagopalan S., Antonia R.A., Turbulence reduction in the mixing layer of a plane jet using small cylinders, Exp. Fluids 25 (1998) 96–103.
[9] Schober M., Fernholz H.-H., Turbulence manipulation in wall jets, in: Gavrilakis S., Machiels L., Monkewitz P.A. (Eds.), Advances in Turbulence, vol. VI, Kluwer, 1996, pp. 529–530.
[10] Vandsburger U., Ding C., Self-excited wire method for the control of turbulent mixing layers, AIAA J. 33 (1995) 1032–1037.
[11] Abrahamsson H., Johansson B., Löfdahl L., A turbulent plane two-dimensional wall-jet in a quiescent surrounding, Eur. J. Mech. B-Fluids 13 (1994) 533–556.
[12] Schober M., Beeinflussung turbulenter Wandstrahlen, Dissertation, Technische Universität Berlin (D 83), and Mensch und Buch Verlag, Berlin, 1999.
[13] Fernholz H.-H., Janke G., Schober M., Wagner P., Warnack D., New developments and applications of skin-friction measuring techniques, Meas. Sci. Technol. 7 (1996) 1396–1409.
[14] Schober M., Grewe F., Fernholz H.-H., Turbulence control in wall jets: a visualisation study, Int. J. Fluid Dyn. 3 (1999) Article 1.
[15] Michalke A., On spatially growing disturbances in an inviscid shear layer, J. Fluid Mech. 23 (1965) 521–544.
[16] Eriksson J.G., Karlsson R.I., Persson J., An experimental study of a two-dimensional plane turbulent wall jet, Exp. Fluids 25 (1998) 50–60.
[17] Abrahamsson H., On a two-dimensional wall-jet, Thesis for degree of licentiate of engineering, Chalmers University of Technology, Göteborg, 1993.
[18] Narasimha R., Narayan K., Parthasarathy S., Parametric analysis of turbulent wall jets in still air, Aeronaut. J. 777 (1973) 335.
[19] Tritton D.J., Physical Fluid Dynamics, Oxford Sci. Publ., 1988.
[20] Koch W., Local instability characteristics and frequency determination of self excited wake flows, J. Sound Vibr. 99 (1985) 53–83.
[21] Monkewitz P.A., The absolute and convective nature of instability in two-dimensional wakes at low Reynolds numbers, Phys. Fluids 31 (1988) 999–1006.
[22] Michalke A., On the inviscid instability of a free-shear layer with wake, Private communication, 1997.
[23] Fernholz H.-H., Finley P.J., The incompressible zero-pressure-gradient turbulent boundary layer: An assessment of the data, Prog. Aerospace Sci. 32 (1996) 245–311.
[24] Johannsson A.V., Alfredsson P.H., Effects of imperfect spatial resolution on measurements of wall-bounded turbulent shear flows, J. Fluid Mech. 137 (1983) 409–421.
[25] Launder B., Rodi W., The turbulent wall jet, Prog. Aerospace Sci. 19 (1981) 81–128.
[26] Blevins R.D., Flow-induced Vibration, Van Nostrand Reinhold Company, 1977.